



Article citation info:

Wen S, Du L, Kong Q, Zhang M, Ding X, Study on Microwave- X assisted TBM Double-edged Cutter Rock-breaking Efficiency and its Positional Relationship, *Eksploracja i Niezawodność – Maintenance and Reliability* 2024: 26(2) <http://doi.org/10.17531/ein/186447>

Study on Microwave-assisted TBM Double-edged Cutter Rock-breaking Efficiency and its Positional Relationship

Indexed by:



Sen Wen^a, Lin Du^a, Qingmei Kong^{a,*}, Min Zhang^a, Xinru Ding^a

^a School of Civil and Architecture Engineering, Henan University, China

Highlights

- Establishing a microwave-assisted TBM double-edged cutter rock-breaking model based on the discrete element method, and exploring the crack propagation mechanism.
- Exploring the positional relationship between microwave waveguides and disc cutters, and proposing the optimal rock-breaking combination mode, further improving the microwave-assisted disc cutter rock-breaking mechanism.

Abstract

In this study, based on a microwave test, the discrete element program (PFC) is used to establish a microwave-assisted disc cutter rock-breaking model and explore the influence law of the positional relationship between microwave radiation and disc cutter penetration on rock-breaking efficiency, and the results show that: The improvement of the positional relationship has a significant effect on improving the rock-breaking efficiency, and the double-edged cutter reaches and minimum rock-breaking specific energy when breaking the rock in the center position with a waveguide spacing of 90 mm and in the inner and outer positions with a waveguide spacing of 150 mm; When the waveguide spacing is 150mm, the double-edged cutter with cutter spacing of 110mm, 130mm, and 190mm have their advantages in rock-breaking efficiency and economic benefits, which should be selected according to the actual needs of the project. The follow-up research should also fully consider the rock type, microwave parameters, cutter profile, engineering environment, and other factors for in-depth investigation.

Keywords

microwave-assisted rock-breaking, double-edged cutter, discrete element, specific energy; positional relationship

This is an open access article under the CC BY license (<https://creativecommons.org/licenses/by/4.0/>)

1. Introduction

With the development of science and technology, TBM (Tunnel Boring Machine) through continuous upgrading and improvement of the tunneling, support, slagging, and other construction processes are integrated and continuous operation, now has a high degree of mechanization, high-efficiency rock-breaking, safety and reliability, green environmental protection, etc., in the field of transportation, water conservancy, and hydropower, municipal tunneling projects are widely used [1]. However, when breaking hard rock strata, the traditional mechanical rock-breaking method has the defect of serious wear

and tear of the disc cutter, which directly leads to higher maintenance costs of machinery, low digging efficiency, prolonged construction period, and a substantial increase in the total economic investment [2-3]. For example, in China Qinling Tunnel Project [4] and Yangtai Mountain Tunnel Project [5], the loss of disc cutter reaches 2.3 m/cutter and 5.4 m/cutter, respectively, while the inspection and replacement of tools and maintenance of cutters and other operations account for about one-third of the total time of the tunneling construction; The disc cutter breaking rates in Kiena gold mine in Canada [6] and

(*) Corresponding author.
E-mail addresses:

S. Wen (ORCID: 0000-0002-9733-3009) 10160063@vip.henu.edu.cn, L. Du 156284918@qq.com, Q. Kong (ORCID: 0009-0002-1166-4251) 10160004@vip.henu.edu.cn, M. Zhang minzhang@henu.edu.cn, X. Ding 769307257@qq.com

Corbalis to Fox mill water main project in USA [7] were 5.6 m/day and 3.7 ~ 4.0 m/day, respectively. To solve this problem, scholars at home and abroad have explored how to transform the traditional rock-breaking method and put forward a variety of auxiliary rock-breaking methods. Among them, the high-pressure water jet method [8-9], laser method [10-11], and high-pressure liquid nitrogen jet method [12-13] can reduce the force of disc cutter rock-breaking and improve the efficiency of rock-breaking when assisting TBM disc cutter rock-breaking, but at the same time, there are defects of the technology itself and the limitations of the environment. The high-pressure water jetting method requires high reliability of hydraulic components, and is easy to cause water accumulation, affecting the construction [14]; The laser method has a small damage range and depth to the rock, and the auxiliary effect is most obvious only when breaking the surface of the rock [15]; the high-pressure liquid nitrogen jet method has a significant effect on the cold impact fracturing of high-temperature rocks in thermal reservoirs, but the effect is poor in other applications, especially in water-bearing formations [16].

Microwave is an electromagnetic wave with a frequency in the range of 300 MHz ~ 300 GHz, which is able to generate thermal energy by causing vibration and friction of polar molecules, and has the characteristics of rapid heating, advanced process, easy to control, safe and harmless, and selective heating [17], which is studied in the field of agroforestry sciences as an important means of food processing [18], material storage [19], and plant refining and optimization [20-22]. Microwave radiation not only has a significant effect on hard rock damage weakening, but also has strong adaptability to the construction environment, and good synergy with TBM and other rock-breaking machinery. Therefore, it attracts many scholars to further explore this. Some scholars have carried out a lot of research in microwave radiation rock damage destruction mechanism. Different rock minerals in the microwave radiation heating effect are different, so the rock in the radiation region forms a large temperature gradient and thermal stress, resulting in rock damage [23][24]. Therefore, the variability of the wave-absorbing capacity of rock minerals is the fundamental cause of damage destruction of rocks due to microwave radiation. Ford et al. [25], Lu et al. [26], and Zheng et al. [27] characterized by dielectric properties and classified them

into strong wave-absorbing minerals, moderately wave-absorbing minerals, and weakly wave-absorbing minerals according to the magnitude of the loss factor; Ali et al. [28], Chen et al. [29], Gautam et al. [30], Lu et al. [31], Sun et al. [32] analyzed from the microscopic point of view and found that the formation of a more pronounced temperature gradient, intergranular cracks, and intragranular cracks successively begin to develop and form crack networks in the process of microwave radiation; Gao et al. [33], and Lu et al. [34] analyzed from a macroscopic point of view and found that the damage to rocks by microwave radiation is mainly manifested as fracture damage and high-temperature melting and that the rock cracks expand radially from the approximate center of the microwave-radiated surface. In addition, the vapor pressure from pore water vaporization under microwave radiation [35][36] and rock mineral phase changes [37][38] contribute to further rock fragmentation.

There are also some scholars from the microwave action mode considerations, to explore the change rule of rock physical and mechanical properties. Through different microwave power and radiation time on the heating damage to a variety of rock specimens, Bisai et al. [39], Deyab et al. [40], Nekoovaght et al. [41], Kahraman et al. [42], and Zheng et al. [43] compared and analyzed the trend of compressive strength and tensile strength of rocks before and after the microwave and showed that with the increase of microwave power and radiation time, the weakening effect of compressive strength and tensile strength gradually increases, and under the same energy, the microwave with "high power and short time" has a better damage effect on the rock; Li et al. [44], Lu et al. [45], Ge et al. [46], Yang et al. [47], and Bai et al. [48] comparatively analyzed the fracture toughness and resistance index (CAI) of rocks before and after microwave and showed that the fracture toughness and resistance index (CAI) of rocks decreased exponentially with the increase of microwave power and radiation time. The change of waveguide position leads to the change of electromagnetic field distribution, which affects the rock warming and damage effects. Ahmadihosseini et al. [49], Hassani et al. [50], Teimoori et al. [51], and Shadi et al. [52] analyzed the effect of microwave radiation by varying the distance between the microwave waveguide and the rock and showed that there are different optimum distances between the waveguide and different types of rocks, mainly related to the real part of the rock dielectric constant; Gao et al.

[53], and Feng et al. [54] also considered and analyzed the effects of multi-waveguide cyclic radiation and rotating waveguide radiation on the rock-breaking effect, respectively. In addition, some scholars combine microwave radiation with disc cutters to explore and analyze. Rui et al. [55] implemented the numerical simulation of microwave-assisted TBM disc cutters breaking by electromagnetic-thermal-force coupling method, and proved that mobile microwave irradiation can better reduce the normal force of disc cutters than fixed microwave irradiation; Lu et al. [56] [57] carried out disc cutters breaking tests on rocks before and after microwave, and the comparative analysis found that: microwave-assisted can reduce the wear of disc cutters and increase the volume of rock-breaking, and the increase of microwave power and radiation time makes the effect of rock-breaking more significant; Hartlieb et al. [58] analyzed the microwave-assisted disc cutter rock-breaking tests and found that microwave radiation increases the rock-breaking efficiency while leading to a larger size of the rock mass broken by the disc cutters.

Previous research on microwave-assisted rock-breaking mainly analyzed the damage mechanism, physical and mechanical property changes, and the effect of disc cutter rock-breaking, but did not consider the relative position of microwave radiation and disc cutter penetration on the disc cutter load changes, crack expansion characteristics, disc cutter rock-breaking efficiency of the impact of the study. Meanwhile, a disc cutter is a tool with an interchangeable rim, usually with single, double, and multiple edges. The study selects a double-edged cutter as the research object, based on the temperature change, strength damage, and crack expansion of granite before and after microwave radiation, and uses the discrete element procedure PFC to establish the microwave-assisted double-edged cutter rock-breaking model. From the point of view of normal force, crack extension characteristics, rock-breaking area, and rock-breaking specific energy, to explore and analyze the influence of the positional relationship between microwave radiation and disc cutter penetration on the performance of microwave-assisted disc cutter rock-breaking, and to put forward the optimal positional relationship of the action from the aspect of rock-breaking efficiency and economic benefits, so as to provide the theoretical basis for the mechanical construction of microwave-assisted TBM disc cutter rock-

breaking technology.

2. Experimental study

2.1. Material characteristics

The high-strength granite from Jining, Shandong Province was selected as the research object, and the mineral composition and content of the rock were examined by petrographic test and XRD diffraction test. The test results show that the granite is mainly composed of potassium feldspar, diopside and biotite, with mineral contents of 69.1%, 26.2% and 4.7%, respectively. The results of petrographic analysis and XRD mapping are shown in Fig. 1 and Fig. 2.

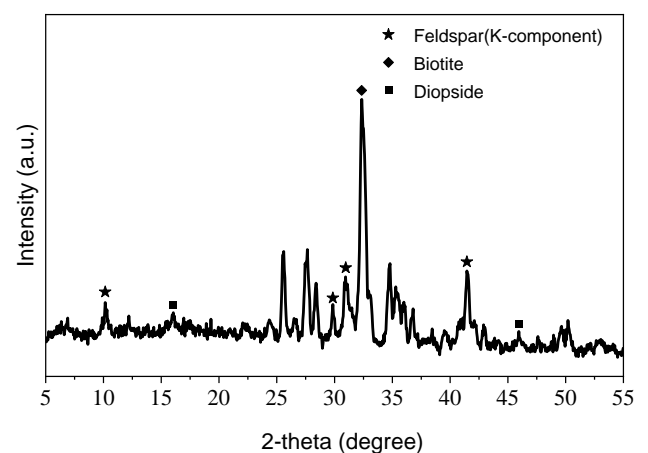


Fig. 1. The XRD analysis results of the granite powder.

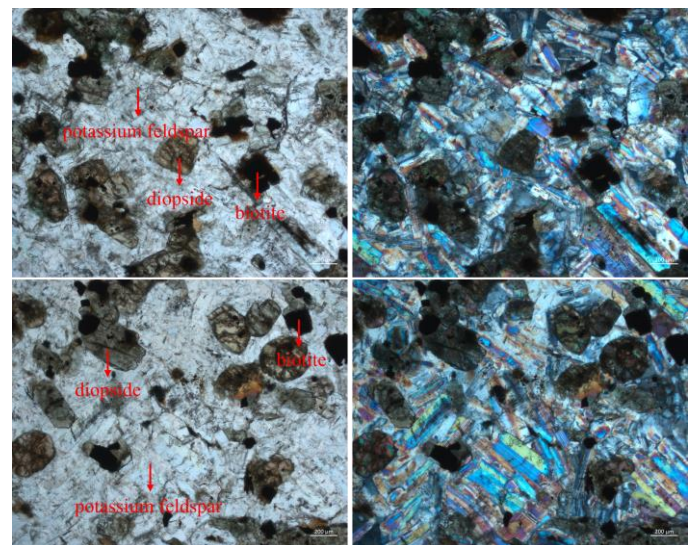


Fig. 2. Petrographic analysis results.

To calculate the penetration depth of microwave radiation into the granite, the dielectric properties of a circular specimen of dried granite with a diameter of 20 mm and a thickness of 3 mm were examined using a vector network analyzer, and the complex dielectric constants at a frequency of 2.45 GHz were

obtained as shown in Table 1. The dielectric constant is the measure of how well a dielectric material responds to microwave radiation as shown in Eq. (1~2) [59].

$$\varepsilon = \varepsilon' - j\varepsilon'' \quad (1)$$

$$\tan \delta = \frac{\varepsilon''}{\varepsilon'} \quad (2)$$

where ε is the relative dielectric constant; the real part; ε' is the permittivity of the material (relative to that of free space); the imaginary part; ε'' is its dielectric loss factor (also relative to ε_0 of free space).

Table 1. The dielectric constant of granite at 2.45 GHz.

Rock samples	ε'	ε''	$\tan\delta$
granite	1.774	0.425	0.239

When the microwave radiation rock, with the increase of penetration depth, microwave energy gradually decreases. In the international community, microwave energy is considered to have ceased to propagate when it decays to 38.6% of the energy of the surface of the medium or $1/e$ ($e=2.718$). According to Eq. (3) [60], the theoretical penetration depth of microwave irradiation granite is calculated as 61.13 mm.

$$Z = \frac{\lambda_0 \sqrt{\varepsilon'}}{2\pi \varepsilon''} \quad (3)$$

where λ_0 is the microwave wavelength.

2.2. Microwave experiment

The test selected a Webox-A9 type microwave heating system for microwave heating of rock samples, which adopts a multimode resonant cavity with a microwave frequency of 2.45GHz, mainly composed of a control box, a microwave generator, and a microwave oven body, as shown in Fig. 3. The set power is 5kW, and the microwave heating is carried out on

the standard granite specimens of $\phi 50 \times 50$ mm and $\phi 50 \times 100$ mm by continuous heating, and the radiation time is 0s, 60s, 120s, 180s, 300s and 420s, respectively. After the microwave radiation is completed, the surface temperature of the rock samples is determined immediately by using the infrared thermometer. After cooling to room temperature, the rock samples were then tested for strength. The microwave test did not consider the effect of pore water in the rock samples, so the rock samples were placed in a drying oven set at 60°C for 48h before the microwave test.

Through the microwave test, it was found that there was no obvious change on the surface of the rock samples within the range of 180s of microwave radiation. When the microwave radiation 180s, the measured average surface temperature of the rock samples 436.8°C ; when the microwave radiation 300s, the measured average surface temperature of the rock samples 578.8°C , and there is obvious damage cracks; when the microwave radiation 420s, the measured average surface temperature of the rock samples 665.3°C , while the internal melting point, the phenomenon of hot melting and along the cracks overflow, and when it cools down is black and hard, as shown in Fig. 4. The surface temperature and mechanical strength of the rock samples were detected and found that: with the increase of microwave radiation time, the surface temperature of the granite gradually increased, and the compressive strength and tensile strength gradually decreased. The results of the surface temperature and mechanical strength of the rock samples before and after microwave are shown in Fig. 5 and Fig. 6 (after 180s of microwave radiation, the surface of the rock samples is obviously damaged, and it is not possible to test its strength).



Fig. 3. Exterior and interior view of the Webox-A9 microwave heating system.

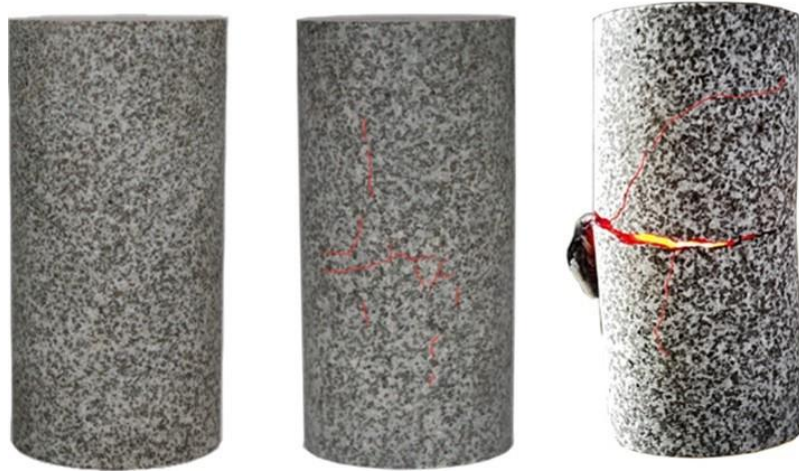


Fig. 4. Microwave power 5kW radiation 0s, 300s, 430s of granite damage patterns.

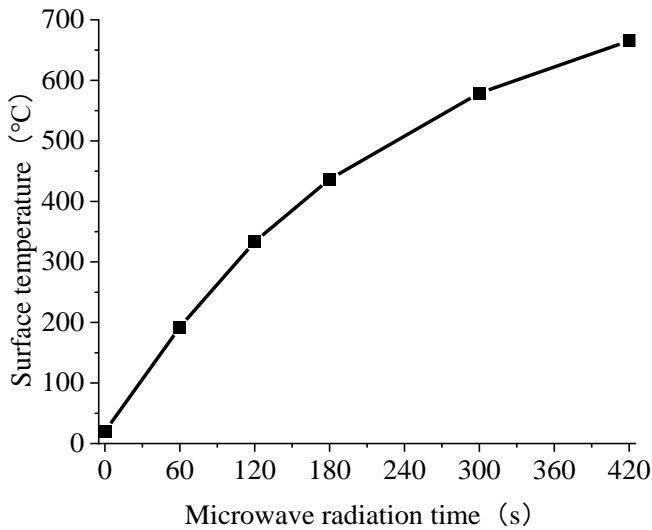


Fig. 5. Rock surface heating with 5kW microwave power.

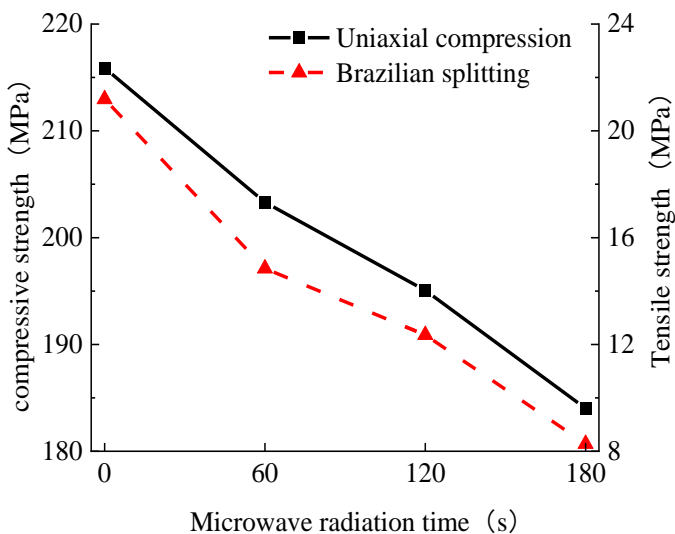


Fig. 6. Rock strength deterioration with 5kW microwave power.

3. Numerical simulation analysis

3.1. Theoretical equations

3.1.1. Simulation calculation equations

The energy absorbed per unit volume of medium in a microwave field can be mathematically represented as follows^[61]:

$$P_d = 2\pi f \epsilon_0 \epsilon'' E_0^2 \quad (4)$$

where P_d is the loss power density deposited within the sample in watts (W/m^3); f is the microwave frequency in hertz(Hz); ϵ_0 is the permittivity of free space($8.85 \times 10^{-12} F/m$); E_0 is the electric field strength.

Assuming that all microwave energy is absorbed by the rock, the energy relationship between the microwave test and the microwave simulation is expressed as:

$$P \times t' = P_d \times t \times V \quad (5)$$

where P is the microwave power(W); t' is the radiation time in the microwave test(s); t is the radiation time in the microwave simulation(s); V is the rock volume of microwave radiation(m^3).

Assuming that the effect of strain change on temperature is negligible, the heat transfer equation for a continuous medium is:

$$-\frac{\partial q_i}{\partial x_i} + P_d = \rho_t C_v \frac{\partial T}{\partial t} \quad (6)$$

where q_i is the heat-flux vector(W/m^2); ρ_t is the mass density(kg/m^3); C_v is the specific heat at constant volume[$J/(kg \cdot ^\circ C)$]; T is the temperature($^\circ C$).

Fourier's law for a continuum establishes the correlation between the heat-flux vector and the temperature gradient as follows:

$$q_i = -k_{ij} \frac{\partial T}{\partial x_j} \quad (7)$$

where k_{ij} is the thermal-conductivity tensor [$W/(m \cdot ^\circ C)$].

Calculation of the thermal expansion effect of continuous media:

$$\Delta R = \alpha R \Delta T \quad (8)$$

where ΔR is the Particle radius increment; α is the coefficient of linear thermal expansion associated with the particle $1/^\circ C$; R is the Particle radius; ΔT is the temperature increment.

Calculation of normal bond damage between continuous media:

$$\Delta \bar{F}_i^n = -\bar{k}_n A \Delta U_n n_i = -\bar{k}_n A \bar{\alpha} \bar{L} \Delta T \quad (9)$$

where \bar{k}_n is the bond's normal stiffness; A is the area of the bond cross-section; $\bar{\alpha}$ is the expansion coefficient of the bond material; \bar{L} is the bond length.

3.1.2. Data processing equations

Calculation of the average normal force reduction of double-edged cutter before and after microwave radiation:

$$\text{Average normal force reduction} = \frac{\bar{F}(p,s) - \bar{F}'(p,s)}{\bar{F}(p,s)} \times 100\% \quad (10)$$

where $\bar{F}(p,s)$ represents the average normal force at the penetration of p mm and a cutter spacing of s mm; $\bar{F}'(p,s)$ represents the average normal force at the penetration of p mm and a cutter spacing of s mm. ($p=\{4,6,8,10,12\}$; $s=\{60,90,120,150,180\}$)

Calculation of specific energy for rock-breaking with the double-edged cutter:

$$S_e = \frac{W}{V} = \frac{\sum_{i=1}^n F_v(i) \cdot d(i)}{V} \quad (11)$$

where W is the energy consumption of the double-edged cutter; V is the rock-breaking volume; n is the analysis step; $F_v(i)$ is the average value of the normal force of the double-edged cutter in the i -th analysis step; $d(i)$ is the normal displacement value of the rolling tool in the i -th analysis step.

Calculation of the specific energy reduction of rock-breaking with double-edged cutters before and after microwave radiation:

$$\text{Rock-breaking specific energy reduction} = \frac{S_e(p,s) - S_e'(p,s)}{S_e(p,s)} \times 100\% \quad (12)$$

where $S_e(p,s)$ represents the specific energy at the penetration of p mm and cutter spacing of s mm; $S_e'(p,s)$ represents the specific energy at the penetration of p mm and

cutter spacing of s mm. ($p=\{4,6,8,10,12\}$; $s=\{60,90,120,150,180\}$)

3.2. Numerical modeling and parameter calibration

As shown in Fig. 7, Granite models with dimensions of 800 mm \times 250 mm and a pore ratio of 0.12 were built by a discrete element procedure and consisted of potassium feldspar (69.1%), diopside (26.2%), and biotite (4.7%), which were characterized using light grey, dark grey and black, respectively. The double-edged cutter has a blade width and edge angle of 15 mm and 20° , respectively, generated by the wall command, and is rigid overall. As shown in Fig. 8, the simulation study of microwave-assisted disc cutters for rock-breaking starts with the use of double waveguides to weaken the rock, followed by the use of a double-edged cutter to break the rock.

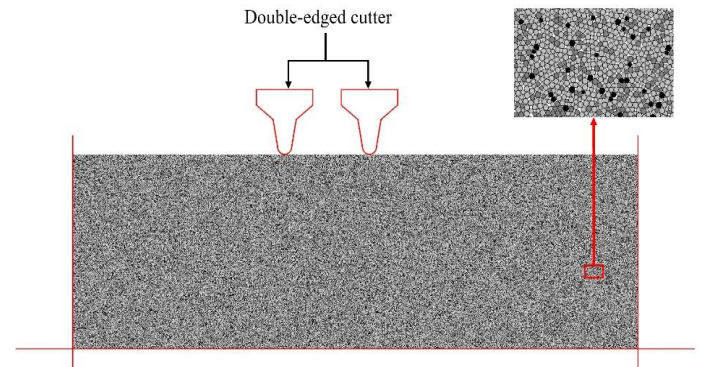


Fig. 7. Rock-breaking model with double-edged cutter.

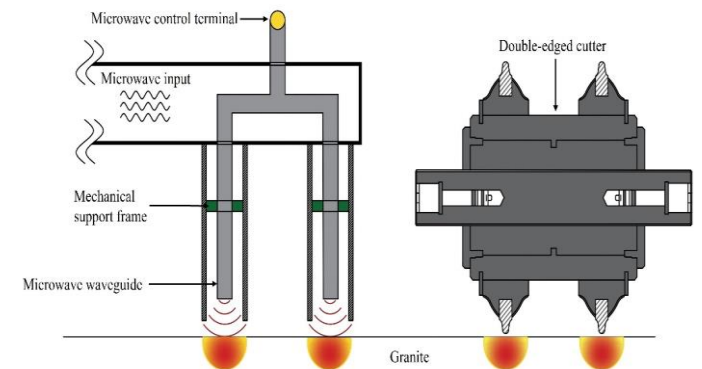


Fig. 8. Schematic diagram of microwave-assisted TBM double-edged cutter breaking.

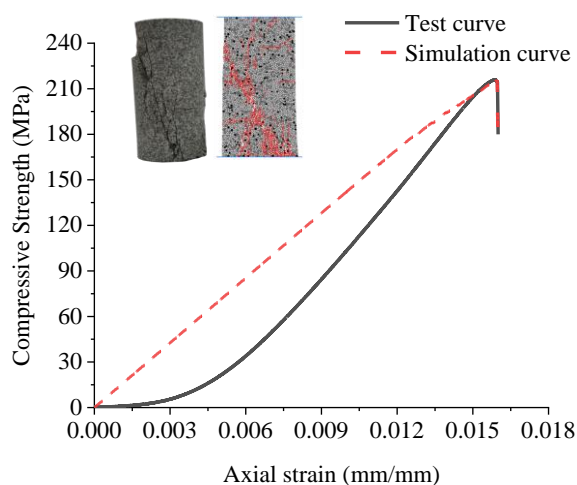
The contact type of the model was selected as parallel bonding, and according to the macro-mechanical parameters, the "trial and error method" was used to calibrate the granite model's microscopic parameters, and the results were shown in Table 2.

Table 2. Microscopic parameters of granite model [26].

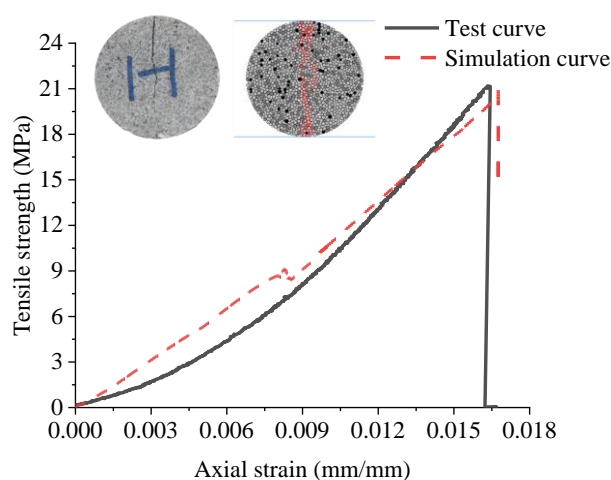
Model variable	Potassium feldspar	Diopside	Biotite
Minimum particle radius/mm		0.5	
Particle size ratio		1.66	
Particle density/kg·m ⁻³	2750	3560	3080
Particle modulus/GPa		12.8	
Particle stiffness ratio		1.5	
Friction coefficient		1.6	
Parallel bonding modulus/GPa		12.8	
Parallel bonding stiffness ratio		1.5	
Parallel bonding normal strength/MPa		108.8±5	
Tangential strength of parallel bonding/MPa		112.5±5	
Thermal expansion coefficient/(10 ⁻⁶)	4.8	6.5	8.3
Thermal conductivity/(W/(m·°C))	2.31	5.76	1.17
Specific heat capacity/(J/(kg·°C))	710	800	760

Eq. (4) serves as a bridge between the electromagnetic and temperature fields, allowing microwave radiant heating to be realized in discrete elements. Considering that the unfolding microwave test energy loss in the microwave cavity with the effect of isolation and reflection of microwaves is relatively small, this study assumes that all the microwave energy is absorbed by the rock, and applies microwave energy to the radiating region based on the principle that the microwave

energy of numerical simulation is equal to the microwave energy of the physical test. Through the microwave test results show that: the use of 5kW microwave power radiation, the increase in radiation time makes the surface temperature of the rock samples rise rapidly, the compressive strength and tensile strength gradually decreased. Due to the rock samples are destroyed after 180s of microwave radiation, it is no longer possible to provide an auxiliary role for the double-edged cutter to break the rock, so the microwave power of 5kW is chosen to radiate the heating and damaging effect of the rock specimen for the 180s as an example to carry out the simulation study of assisted double-edged cutter breaking. Calculated by Eq. (5), simulation uses microwave power density of 1×10^{10} W/m³ radiated 0.018s and 0.046s for standard granite samples subjected to uniaxial compression and Brazilian splitting, respectively. Complete the theoretical calculation of heat conduction and bonding damage according to Eq. (6) ~ (9). The comparison of the results of the mechanical test and numerical simulation is shown in Fig. 9 and Table 3, the relative errors of elastic modulus, Poisson's ratio, compressive strength, and tensile strength before and after microwave are below 3%, and the simulation results of microwave -irradiated rock samples are consistent with the results of the indoor test in the aspects of strength weakening, temperature growth, crack development pattern and indicates that the calibration of fine-scale parameters is more accurate and the simulation results are reasonable.



a



b

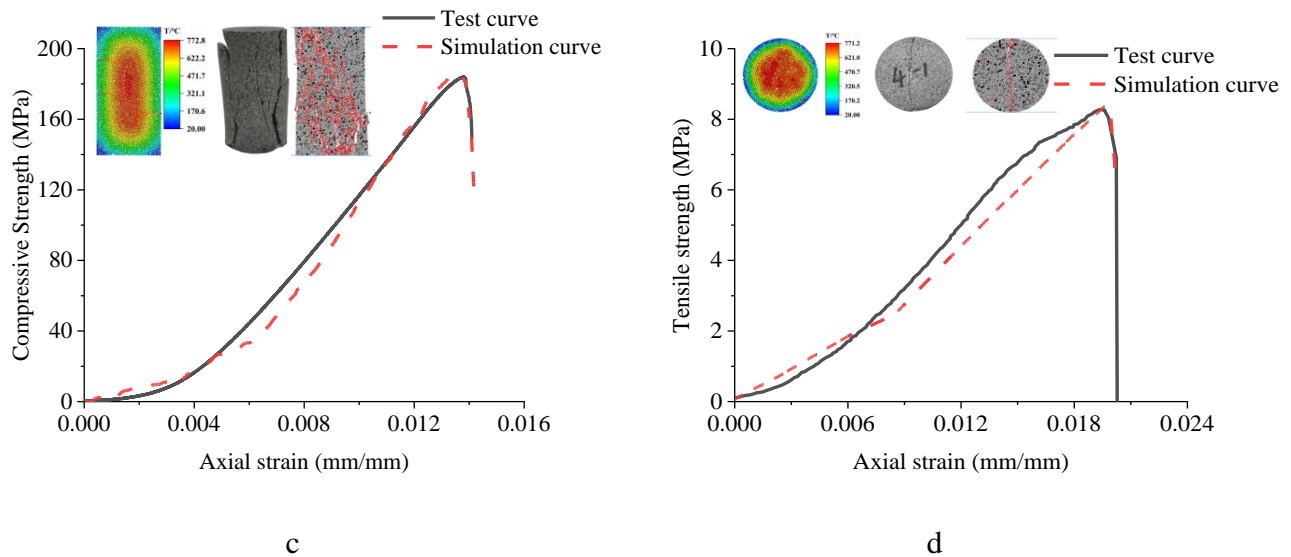


Fig. 9. Comparison of experimental and simulated stress-strain curves: (a) Uniaxial compression before microwave radiation; (b) Brazil splitting before microwave radiation; (c) Uniaxial compression after microwave radiation; (d) Brazilian splitting after microwave radiation.

Table 3. Comparison between experimental results and numerical simulation results.

	Before microwave radiation				Microwave power 5kW radiation for 180s			
	E/GPa	ν	Sc/MPa	St/MPa	E/GPa	ν	Sc/MPa	St/MPa
Laboratory test	19.35	0.336	215.88	21.185	18.38	0.193	184.012	8.277
Numerical simulation	19.39	0.341	215.653	21.14	18.91	0.198	185.560	8.440
Relative error	0.21%	1.50%	0.11%	0.21%	2.88%	2.59%	0.84%	1.97%

The international standard WR340 type waveguide with a width of 43.18 mm was selected for the simulation, and its applicable frequency range (2.20 GHz to 3.30 GHz) meets the requirements for the use of the required microwave frequency (2.45 GHz). The theoretical penetration depth of 61.13 mm for microwave radiated granite has been calculated and obtained according to Eq. (3). Since the extent of microwave action on the same horizontal plane decreases with increasing radiation depth, the radiation area is set to be semi-elliptic^[62]. Calculated by Eq. (5), the microwave power density of 1×10^{10} W/m³ should be used to radiate 0.043s to the granite in this area, and the effect of microwave radiation is shown in Fig. 10.

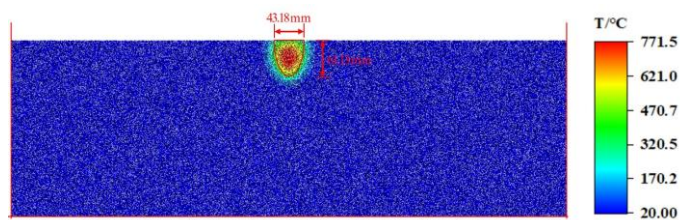


Fig. 10. Microwave radiation effect.

The initial temperature of the rock is 20°C, and the microwaves form a maximum temperature of 771.5°C at the

center of the rock's radiation area, decreasing in all directions.

3.3. Research programme

The study used double waveguides for microwave radiation heating of the rock and divided the two microwave radiation heating intervals in the rock into four equal segments, taking the middle three points from the inside to the outside of the correspondingly labeled as the inner position, the center position, and the outer position, respectively. The rock model has a peripheral pressure of 5 MPa, and the double-edged cutter penetrates the rock at a speed of 0.1 m/s. To investigate the effect of a microwave-assisted double-edged cutter on rock-breaking, comparative analysis of rock breakage before and after microwave radiation was carried out using a double-edged cutter at the center of waveguide spacing of 60mm, 90mm, 120mm, 150mm, and 180mm. Considering that the distance of the inner position at the waveguide spacing of 60 mm is too close, it is difficult to place the double-edged cutter, so to explore the influence of the relative position on the double-edged cutter to break the rock law, the double-edged cutter is compared and analyzed to penetrate the rock only at the relative

positions of the waveguide spacing of 90 mm, 120 mm, 150 mm and 180 mm as shown in Table 4. During the double-edged cutter breaking process, the normal force and specific energy

were recorded and analyzed at 4mm, 6mm, 8mm, 10mm, and 12mm of penetration.

Table 4. The relative position of the microwave and double-edged cutter.

relative position	waveguide spacing			
	90mm	120mm	150mm	180mm
inner position				
center position				
outer position				

3.4. Result analysis

3.4.1. Analysis of the normal force of the double-edged cutter

To analyze the weakening effect of microwave assistance on the normal force of the double-edged cutter to break the rock, the average normal force of the double-edged cutter before and after microwave radiation was recorded and analyzed for different combinations of cutter spacing and penetration during penetration at the center position, as shown in Fig.11. The average normal force of the double-edged cutter before microwave radiation is between $1.747 \text{ MN}\cdot\text{m}^{-1}$ and $6.791 \text{ MN}\cdot\text{m}^{-1}$; the average normal force of the double-edged hob after microwave radiation is between $0.474 \text{ MN}\cdot\text{m}^{-1}$ and $1.505 \text{ MN}\cdot\text{m}^{-1}$. It can be seen that the normal force of the double-edged cutter is obviously weakened under the effect of microwave radiation. The average normal force of the double-edged cutter before and after microwave radiation is the minimum value when the cutter spacing is 60 mm, and it increases gradually with the increase of the cutter spacing. With the increase in penetration, the trend of the average normal force of the double-edged cutter is changed by the influence of microwave radiation. Before microwave radiation, the average normal force of the double-edged cutter decreases with the increase of penetration and tends to stabilize gradually; After

microwave radiation, the average normal force of the double-edged cutter fluctuates up and down with the increase of penetration, with no obvious trend pattern. According to Eq. (10), the reduction of the average normal force of the double-edged cutter before and after microwave radiation is calculated at different combinations of cutter spacing and penetration, and the results are shown in Table 5. From the table, it can be seen that the weakening effect of microwave radiation on the average normal force of the double-edged cutter is significant, and the decrease of the average normal force of the double-edged cutter is more than 61.52% in the range of cutter spacing of 180 mm and penetration of 12 mm. In addition, the changes in cutter spacing and penetration will also affect the weakening effect of the average normal force of the double-edged cutter, with the increase of cutter spacing, the decrease of the average normal force of the double-edged cutter gradually decreases, which is due to the increase of the spacing of the waveguide to weaken the damaging effect of the microwave radiation; with the increase of penetration, the decrease of the average normal force of the double-edged cutter shows a trend of increasing and then decreasing and reaches its maximum in the double-edged cutter penetration of 6mm or 8mm. The decrease in the average normal force of the double-edged cutter is due to the formation of a dense core in the rock-breaking process, which weakens the effect of microwave assistance to a certain extent.

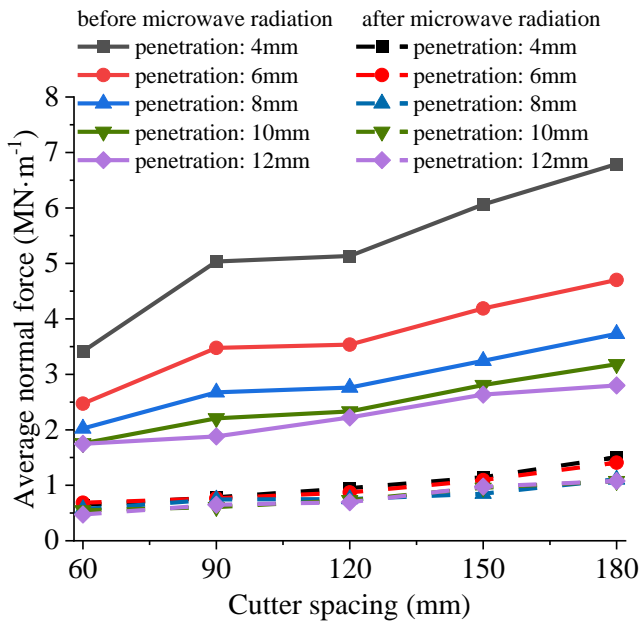


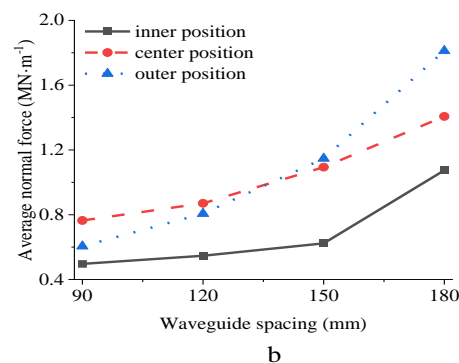
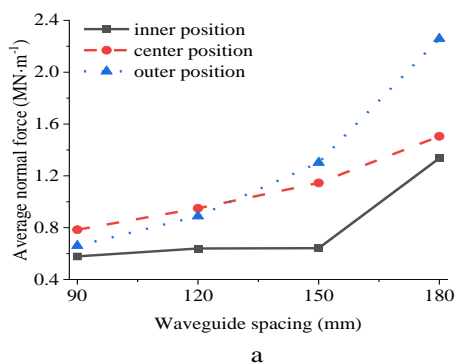
Fig. 11. The change curves of the average normal force of the double-edged cutter at the center position before and after microwave radiation.

Table 5. Average normal force decrease of double-edged cutter before and after microwave radiation.

Penetration	Cutter spacing				
	60mm	90mm	120mm	150mm	180mm
4mm	81.12%	72.29%	71.79%	68.80%	72.87%
6mm	84.43%	78.02%	72.15%	72.53%	65.52%
8mm	81.51%	75.38%	72.77%	68.66%	68.79%
10mm	81.10%	73.88%	73.81%	66.01%	62.96%
12mm	77.84%	70.08%	70.38%	66.22%	61.52%

As to investigate the influence law of the relative positions of microwave and double-edged cutter on the normal force of double-edged cutter breaking, the average normal force change curves of double-edged cutter at three relative positions with different waveguide spacing and penetration are recorded and plotted, as shown in Fig. 12. The average normal force of the double-edged cutter at all three relative positions increases with increasing waveguide spacing within penetration of 12 mm and

waveguide spacing of 180 mm. In the range of waveguide spacing 180mm, the average normal force of a double-edged cutter when breaking rock in the inner position is always smaller than that in the center and outer positions. Within the range of 150 mm waveguide spacing, the average normal force of the double-edged cutter in breaking rock in the inner position grows slowly, and the maximum increase is 14%; while the waveguide spacing is more than 150mm, the increase in penetration of 4 mm, 6 mm, 8 mm, 10 mm, and 12 mm is 108.26%, 72.37%, 67.79%, 57.90%, and 27.36%, respectively, and the inner position of the average normal force of the double-edged cutter increases significantly and the growth decreases gradually with the increase of the penetration. As the waveguide spacing increases, the average normal force growth rate of the double-edged cutter in breaking rock in the outer position is significantly greater than in the center position. When the waveguide spacing is less than 120 mm, the average normal force of the double-edged cutter in the outer position is less than that in the center position; When the waveguide spacing is in the range of 120mm to 150mm, the average normal force of the double-edged cutter in the outer position gradually exceeds that of the double-edged cutter in the center position. When the waveguide spacing is greater than 150 mm, the average normal force of the double-edged cutter in the outer position is greater than that in the center position. The comparison of the average normal force of the double-edged cutter when breaking rock at three relative positions revealed that the maximum average normal force of 2.258 MN·m⁻¹ was achieved when breaking rock at the outer position with waveguide spacing of 180 mm and penetration of 4 mm, and the minimum mean normal force of 0.479 MN·m⁻¹ was achieved when breaking rock at the inner position with waveguide spacing of 90 mm and penetration of 8 mm.



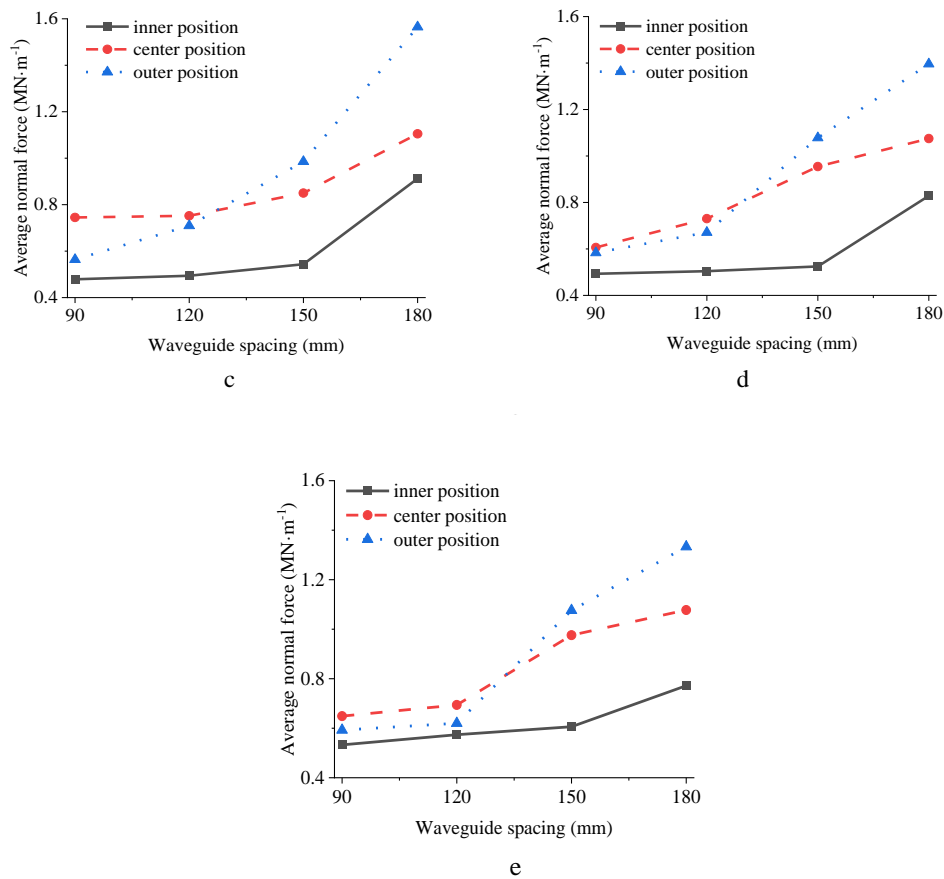
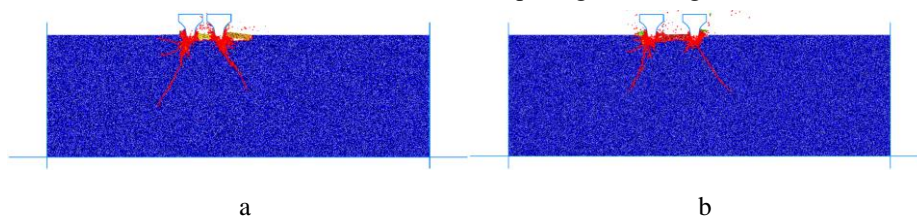


Fig. 12. The change curve of the average normal force of the double-edged cutter in different relative positions: (a) penetration: 4 mm; (b) penetration: 6 mm; (c) penetration: 8 mm; (d) penetration: 10 mm; (e) penetration: 12 mm.

3.4.2. Analysis of rock-breaking crack propagation

Taking the maximum penetration of 12mm as an example, the crack extension mechanism and rock damage characteristics of double-edged cutter breaking at different cutter spacing are analyzed, as shown in Fig. 13. To analyze the rock-breaking situation more intuitively, different colors were used to characterize the broken rock pieces. Among them, the unbroken rocks are characterized by blue color, and the individual rock fragments broken by the double-edged cutter are characterized by different colors. After the double-edged cutter penetrates, the lateral crack expands along the vertical direction of the double-edged cutter penetration, and the length is shorter; the

longitudinal crack expands along the direction of the double-edged cutter penetration, and it is distributed in the shape of Chinese "herringbone". When the cutter spacing is 60 mm, 90 mm, 120 mm, 150 mm, and 180 mm, the rock fragmentation area is $2.429 \times 10^{-3} \text{ m}^2$, $2.883 \times 10^{-3} \text{ m}^2$, $2.038 \times 10^{-3} \text{ m}^2$, $1.983 \times 10^{-3} \text{ m}^2$, $1.865 \times 10^{-3} \text{ m}^2$, respectively. Within the cutter spacing of 90mm, the lateral cracks pass through each other, promoting the spalling of rock between the double-edged cutter, when the cutter spacing of 90mm, the rock has the largest broken area; when the cutter spacing exceeds 120mm, the lateral cracks do not pass through, and the rock is broken only in the area below and on both sides of the double-edged cutter, and the cutter spacing is too large.



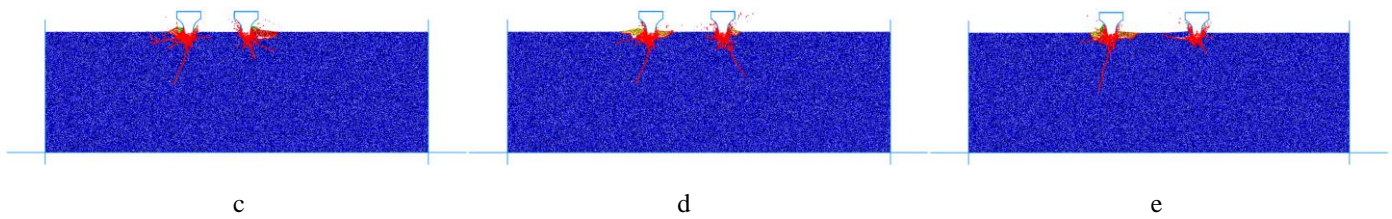
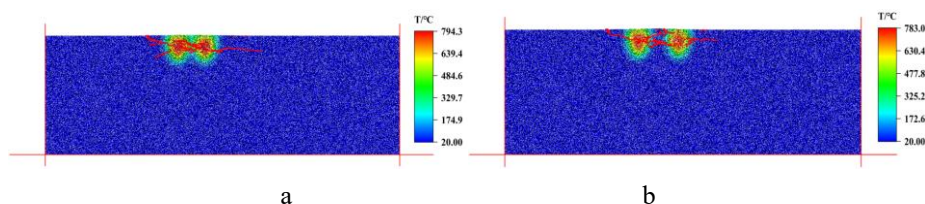


Fig. 13. Crack distribution at different cutter spacing before microwave radiation: (a) cutter spacing: 60mm; (b) cutter spacing: 90mm; (c) cutter spacing: 120mm; (d) cutter spacing: 150mm; (e) cutter spacing: 180mm.

The temperature and crack distribution characteristics formed by the double waveguides using different waveguide spacing for microwave radiation heating of the rock are shown in Fig. 14. When the waveguide spacing of 60mm, 90mm, 120mm, 150mm, and 180mm form the maximum temperature of 794.3°C, 783.0°C, 774.9°C, 774.1°C and 773.4°C, respectively, the maximum temperature of the rock decreases and tends to be stable with the increase of waveguide spacing. Due to the rock except the palm face being surrounded by pressure, the crack extension played a restraining effect, in the thermal expansion and thermal stress, did not produce longitudinal cracks along the direction of the double-edged cutter penetration, but from the thermal core area to form lateral cracks, and along the perpendicular to the direction of the double-edged cutter penetration to the surface of the rock to expand, conducive to the surface of the rock block spalling. Within the range of 150 mm waveguide spacing, the cracks generated by the double waveguides action are connected, and the larger the waveguide spacing is, the closer the connected cracks between the radiating regions are to the surface of the rock; when the waveguide spacing exceeds 150 mm, the cracks generated by the double waveguides action are not connected.

The crack distribution and rock damage characteristics of the double-edged cutter at the center position penetrating 12 mm after microwave action with different waveguide spacing are shown in Fig. 15. Combined with Fig. 13, the comparison found that the cracks generated after the penetration of the double-edged cutter are mainly perpendicular to the direction of the double-edged cutter penetration, which is more conducive to the

promotion of the breaking of the rock between the double-edged cutter, induced by the lateral cracks generated by the microwave radiation. After a waveguide spacing of 150 mm, the effects of thermal damage cracking diminished, producing a small amount of longitudinal cracking in the direction of the double-edged cutter penetration. As shown in Fig. 18, in the range of waveguide spacing from 60mm to 180mm, the rock fragmentation area in the center position shows a trend of "first up and then down" with the increase of waveguide spacing, and the rock fragmentation area reaches the maximum when the waveguide spacing is 90mm. At waveguide spacing of 60 mm, 90 mm, 120 mm, 150 mm, and 180 mm, the breaking area of the double-edged cutter in the center position was $3.266 \times 10^{-3} \text{ m}^2$, $6.802 \times 10^{-3} \text{ m}^2$, $4.862 \times 10^{-3} \text{ m}^2$, $4.438 \times 10^{-3} \text{ m}^2$, $3.456 \times 10^{-3} \text{ m}^2$, respectively. Compared with the rock-breaking by the double-edged cutter with the same cutter spacing before microwave radiation, the rock-breaking area increased by 34.46%, 135.93%, 138.57%, 123.80%, and 85.31%, respectively. It can be seen that the microwave assistance can greatly improve the rock-breaking area, and in the range of waveguide spacing 90mm to 150mm, the extended crack produced by the double-edged cutter penetration in the center position has a significant effect on the breaking effect on the surface of the rock, whereas in the case of the waveguide spacing of 60mm and 180mm, due to the irrational arrangement of the waveguide and the spacing of the double-edged cutter, although it produces a longer lateral crack, it is insufficient in the width and depth of the rock-breaking, resulting in a relatively poor effect of rock-breaking.



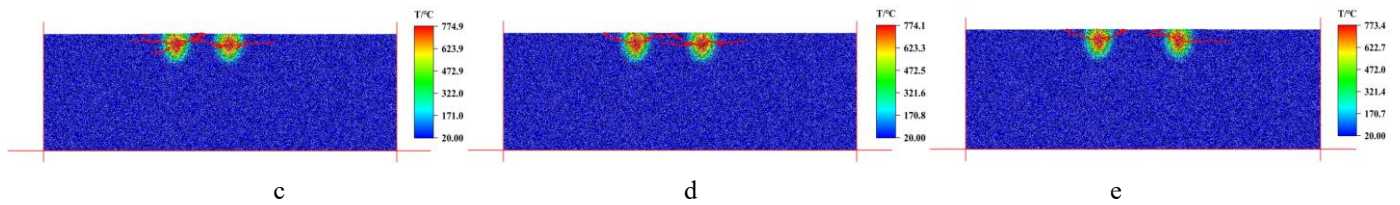


Fig. 14. Temperature and crack distribution in the rock after microwave radiation: (a) waveguide spacing: 60mm; (b) waveguide spacing: 90mm; (c) waveguide spacing: 120mm; (d) waveguide spacing: 150mm; (e) waveguide spacing: 180mm.

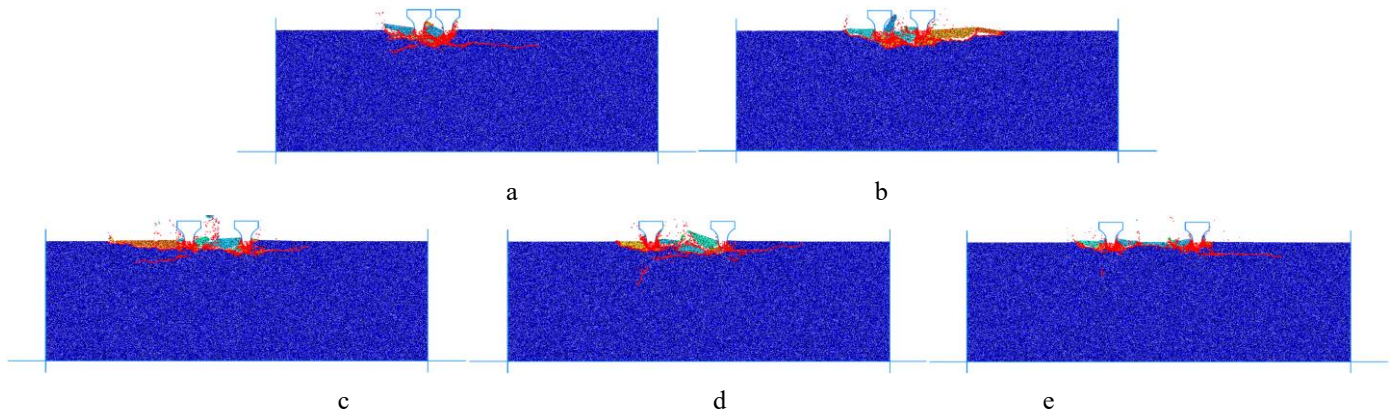


Fig. 15. Crack distribution in the center position of broken rock at different waveguide spacing after microwave radiation: (a) waveguide spacing: 60mm; (b) waveguide spacing: 90mm; (c) waveguide spacing: 120mm; (d) waveguide spacing: 150mm; (e) waveguide spacing: 180mm.

The crack distribution and rock fragmentation characteristics of the double-edged cutter when penetrating 12 mm in the inner and outer positions with different waveguide spacings are shown in Figs. 16 and 17, respectively. Combined with Fig. 18, it is found that the double-edged cutter penetration in the inner and outer positions still produces mainly lateral cracks perpendicular to the direction of double-edged cutter penetration, and the rock fragmentation area in the inner and outer positions has the same trend with the increase of waveguide spacing. When the waveguide spacing is 90mm, due to the close spacing between the waveguide and the double-edged cutter, the lateral crack extension generated by the double-edged cutter penetrating in the inner and outer positions is insufficient, and it mainly breaks the rock between and below the double-edged cutter, and the rock-breaking area is relatively small. With the increase of waveguide spacing, the extension length of lateral cracks to both sides increases, which makes the rock fragmentation area increase gradually. When the waveguide spacing is 150 mm, the rock fragmentation area of the inner and outer positions reaches the maximum value of $7.307 \times 10^{-3} \text{ m}^2$, and $7.221 \times 10^{-3} \text{ m}^2$ respectively. When the waveguide spacing is more than 150mm, the rock crack between the double-edged cutter is not through when the inner position

breaks the rock, and no synergistic rock-breaking is formed, while when the outer position breaks the rock, although the rock crack between the double-edged cutter is through, the depth of the rock-breaking is not enough, the rock-breaking effect is poor, and the broken area is reduced rapidly. When the waveguide spacing is 180 mm, the rock fragmentation area reaches a minimum value of $2.166 \times 10^{-3} \text{ m}^2$, and $4.033 \times 10^{-3} \text{ m}^2$ in the inner and outer positions, respectively. Comparison with the change curves of the rock fragmentation area at the center position reveals that the rock fragmentation area in three relative positions within the range of waveguide spacing from 90 mm to 150 mm is greater than $4.032 \times 10^{-3} \text{ m}^2$, which is a better effect of rock-breaking. Among them, when the waveguide spacing is less than 120mm, the rock fragmentation area of the center position is larger than that of the inner and outer positions; when the waveguide spacing is 150mm, the rock fragmentation area of the inner and outer positions increases rapidly and exceeds that of the center position, reaching the maximum rock fragmentation area.

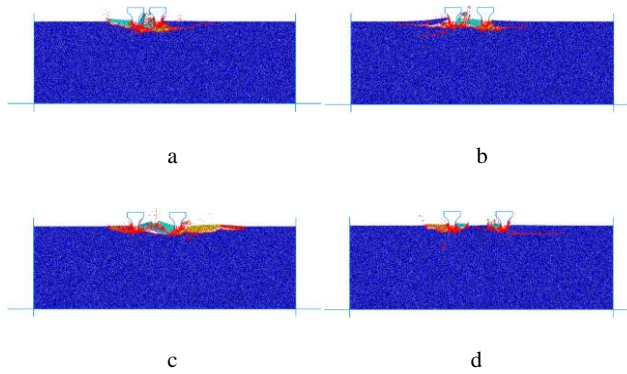


Fig. 16. Crack distribution in the inner position of broken rock at different waveguide spacings after microwave radiation: (a) waveguide spacing: 90mm; (b) waveguide spacing: 120mm; (c) waveguide spacing: 150mm; (d) waveguide spacing: 180mm.

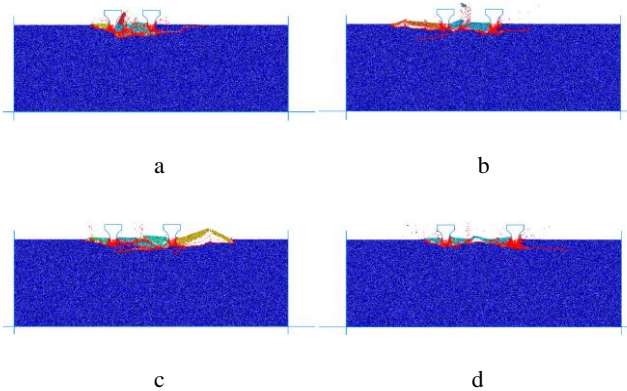


Fig. 17. Crack distribution in the outer position of broken rock at different waveguide spacings after microwave radiation: (a) waveguide spacing: 90mm; (b) waveguide spacing: 120mm; (c) waveguide spacing: 150mm; (d) waveguide spacing: 180mm.

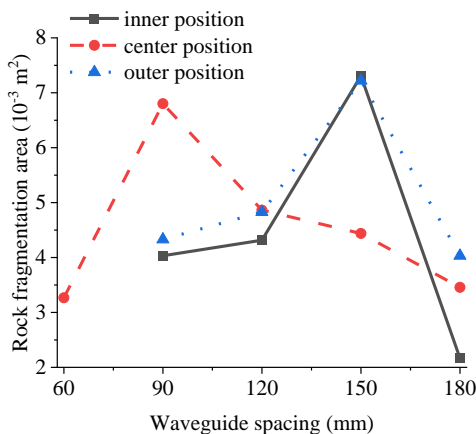


Fig. 18. The change curves of the rock fragmentation area of the double-edged cutter in three relative positions with different waveguide spacings

3.4.3. Analysis of rock-breaking efficiency

To investigate the effect of microwave assistance on the rock-breaking efficiency of the double-edged cutter, the specific energy of rock-breaking of the double-edged cutter is calculated according to Eq. (11), and the change curve of the specific energy of rock-breaking of the double-edged cutter in the center position before and after the microwave radiation is plotted for the comparative analysis, as shown in Fig. 19. In the range of cutter spacing of 180mm and penetration of 12mm, before and after microwave radiation, different penetration of the double-edged cutter rock-breaking specific energy with the increase of the cutter spacing show a "first lower and then higher" trend, when the cutter spacing is 90mm, the rock-breaking specific energy is the smallest. Before microwave radiation, the variation interval of the rock-breaking specific energy of the double-edged cutter is $22.125 \text{ MN}\cdot\text{m}^{-2}$ to $48.900 \text{ MN}\cdot\text{m}^{-2}$, and the variation of the rock-breaking specific energy in the range of 150 mm between double-edged cutter is relatively small, with the variation range of 2.41% to 30.19%; the variation of rock-breaking specific energy is relatively large when the cutter spacing is greater than 150 mm, and the variation ranges from 55.59% to 85.28%. After microwave radiation, the variation interval of the specific energy of double-edged cutter breaking was from $1.836 \text{ MN}\cdot\text{m}^{-2}$ to $8.693 \text{ MN}\cdot\text{m}^{-2}$ and showed a V-shaped trend. The degradation of the specific energy of the double-edged cutter breaking by microwave assistance is calculated according to Eq. (12), as shown in Table 6. In the range of cutter spacing of 180mm and penetration of 12mm, the decrease of rock-breaking specific energy of the double-edged cutter after microwave radiation is between 75.66% and 92.33%, and the decrease of rock-breaking specific energy of different cutter spacings shows the trend of "rising, then decreasing, then rising" with the increase of penetration, and the decrease of rock-breaking specific energy of the double-edged cutter with penetration of 6mm and 12mm is relatively larger. In particular, the reduction of rock-breaking specific energy reaches the maximum when the penetration is 6mm, and the reduction is 90.12%, 88.26%, 92.33%, 88.95%, and 90.51% when the cutter spacing is 60m, 90mm, 120mm, 150mm, and 180mm respectively. It can be seen that the microwave-assisted can greatly reduce the rock-breaking specific energy, and the effect on the improvement of the double-edged cutter rock-breaking

efficiency is significant.

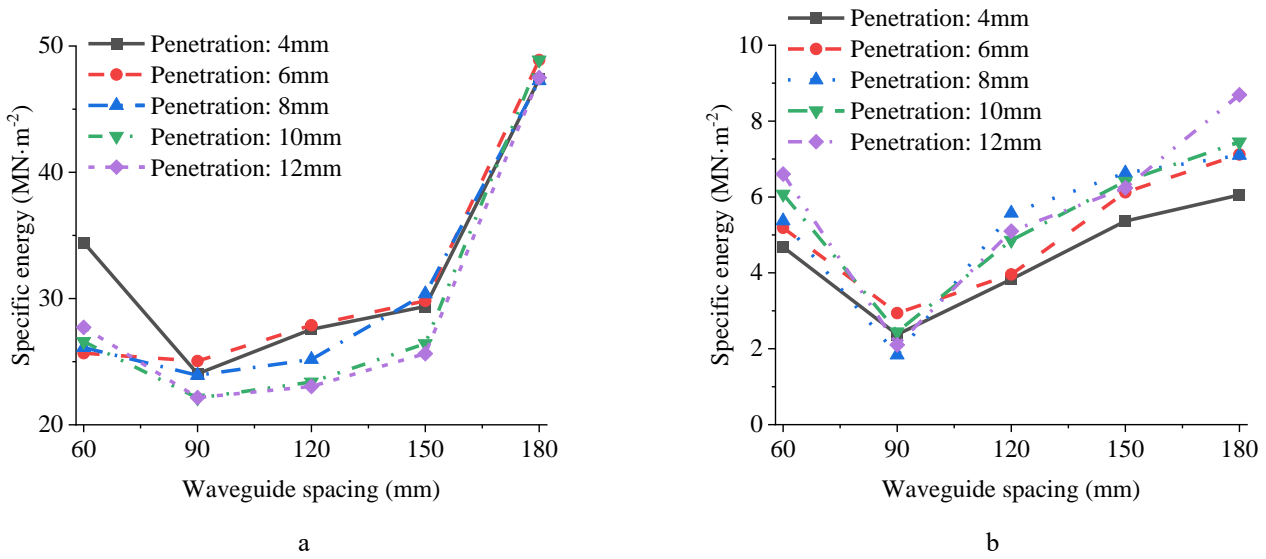


Fig. 19. The change curves of rock-breaking specific energy of double-edged cutter in the center position before and after microwave radiation: (a) before microwave radiation; (b) after microwave radiation.

Table 6. Specific energy reduction of double-edged cutter breaking before and after microwave radiation.

Penetration	Cutter spacing				
	60mm	90mm	120mm	150mm	180mm
4mm	86.42%	79.79%	79.44%	77.15%	76.17%
6mm	90.12%	88.26%	92.33%	88.95%	90.51%
8mm	86.11%	85.81%	77.86%	79.22%	77.87%
10mm	81.74%	79.46%	78.16%	75.73%	75.66%
12mm	87.23%	85.44%	84.98%	84.76%	81.70%

To investigate the influence law of the relative position of microwave and double-edged cutter on the rock-breaking efficiency, the change curves of the double-edged cutter rock-breaking specific energy for three relative positions with different waveguide spacing and penetration are recorded and plotted, as shown in Fig. 20. Combined with Fig. 19(b), it can be seen that: within the range of 12mm penetration, the three relative positions show a trend of "first down and then up" with the increase of waveguide spacing, and in the simulation calculation of the waveguide spacing, the specific energy of the double-edged cutter in the center position of the rock-breaking reaches a minimum when the waveguide spacing is 90mm; the specific energy of the double-edged cutter in the outer position and the inner position of the rock-breaking reaches a minimum when the waveguide spacing of 150mm. The analysis of the rock-breaking specific energy of the three relative positions reveals that when the waveguide spacing is 90mm, the rock-breaking specific energy of the inner position is always smaller

than that of the outer position within the range of penetration of 12mm and the change amplitude is small, with the maximum difference amplitude being 25.01%; the center position has the smallest rock-breaking specific energy, and the magnitude of the difference in rock-breaking specific energy increases gradually from 10.68% to 47.81% with increasing penetration compared to the inner position. In the range of waveguide spacing from 90mm to 150mm, the rock-breaking specific energy of the center position gradually increases, the inner and outer positions gradually decrease, and the rock-breaking specific energies of the waveguide spacing of 120mm and 150mm are the center position, the outer position, and the inner position from large to small, respectively. In the range of waveguide spacing from 150mm to 180mm, the rock-breaking specific energy of the inner and outer positions gradually increases, the growth rate is larger than the rock-breaking specific energy of the center position, and the rock-breaking specific energies of the waveguide spacing of 180mm are the inner position, the outer position, and the center position from large to small, respectively. The comparison of the minimum breaking specific energy of the inner, center, and outer positions in the range of 12 mm of penetration reveals that the average breaking specific energy of the inner position is the smallest, and the average rock-breaking specific energy of the center and outer positions is 14.26% and 21.78% higher than that of the inner position, respectively.

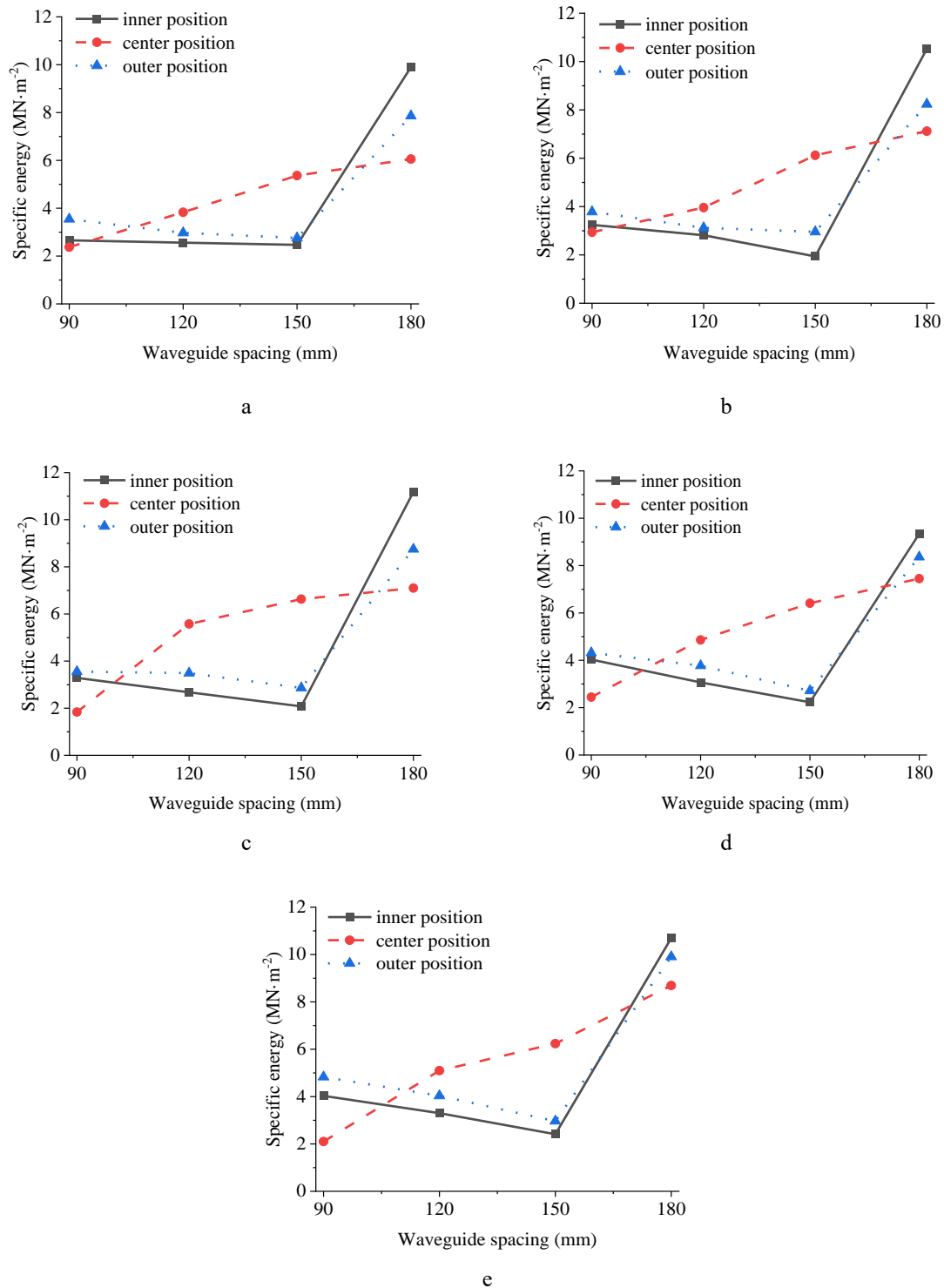


Fig. 20. The change curves of rock-breaking specific energy of double-edged cutter with different relative positions: (a) penetration: 4 mm; (b) penetration: 6 mm; (c) penetration: 8 mm; (d) penetration: 10 mm; (e) penetration: 12 mm.

3.5. Optimal position analysis

Based on the studies of three relative positions of the microwave and double-edged cutter, it is found that when the waveguide spacing is 150 mm, the double-edged cutter achieves the maximum rock fragmentation area and the minimum rock-

breaking specific energy in both the inner position and the outer position. Therefore, a combined rock-breaking simulation study was carried out using a double-edged cutter with different cutter spacings and double waveguides with waveguide spacing of 150 mm to further analyze the optimal position of the microwave and double-edged cutter. The double-edged cutter is

all arranged with the center line between the waveguides as the axis of symmetry, and the cutter spacing is 70mm, 90mm, 110mm, 130mm, 150mm, 170mm, 190mm, 210mm, and 230mm, where 130mm, 150mm, and 170mm are the inner, center, and outer positions of the microwave radiation area, respectively. When the waveguide spacing is 150 mm, the crack distribution and the change curves of the area of broken rock mass at 12 mm penetration of the double-edged cutter with different cutter spacing are shown in Fig. 21 and Fig. 22. Under the influence of microwave radiation, the double-edged cutter with cutter spacing from 70mm to 230mm produces lateral cracks perpendicular to the penetration direction of the double-edged cutter, and when the cutter spacing is 230mm, the damaged cracks in the rock between the disc cutters do not penetrate completely and form rock ridges. Combined with Fig. 23, the change curves of the average normal force and specific energy of rock-breaking of double-edged cutter can be seen: due to the influence of microwave radiation and cutter spacing, the area of broken rock mass, the average normal force of double-edged cutter and specific energy of rock-breaking show up and down oscillatory change trend with the increase of cutter spacing. When the double-edged cutter is on the inner side of the waveguides (cutter spacing less than 150mm), the area of the broken rock mass shows a trend of "decrease, then increase, then decrease again" with the increase of cutter spacing, the average normal force and rock-breaking specific energy show a

trend of "increase, then decrease, then increase" with the increase of cutter spacing, and the average normal force reaches a minimum when the cutter spacing is 110mm and reaches the maximum area of the broken rock mass and the minimum rock-breaking specific energy when the cutter spacing is 130mm; when the double-edged cutter is on the outer side of the waveguide (cutter spacing more than 150mm), the area of the broken rock mass shows the trend of "first increase and then decrease" with the increase of the cutter spacing, the average normal force shows the trend of "first increase and then decrease and then increase" with the increase of the cutter spacing, and the specific energy of the rock breakage shows the trend of "first decrease and then increase" with the increase of the cutter spacing, and when the cutter spacing of 190mm to achieve the maximum area of broken rock, the minimum average normal force and the minimum rock-breaking specific energy. Although the average normal force when the hob breaks rock on the outer side of the waveguide is higher than that on the inner side of the waveguide, the area of rock broken on the outer side of the waveguide is significantly larger than that on the inner side of the waveguide within the cutter spacing of 210 mm. It is calculated that the average normal force of the double-edged cutter reaches the minimum when the cutter spacing is 110mm; the rock-breaking specific energy can reach the minimum when the cutter spacing is 130mm; the rock-breaking area reaches the maximum when the cutter spacing is 190mm.

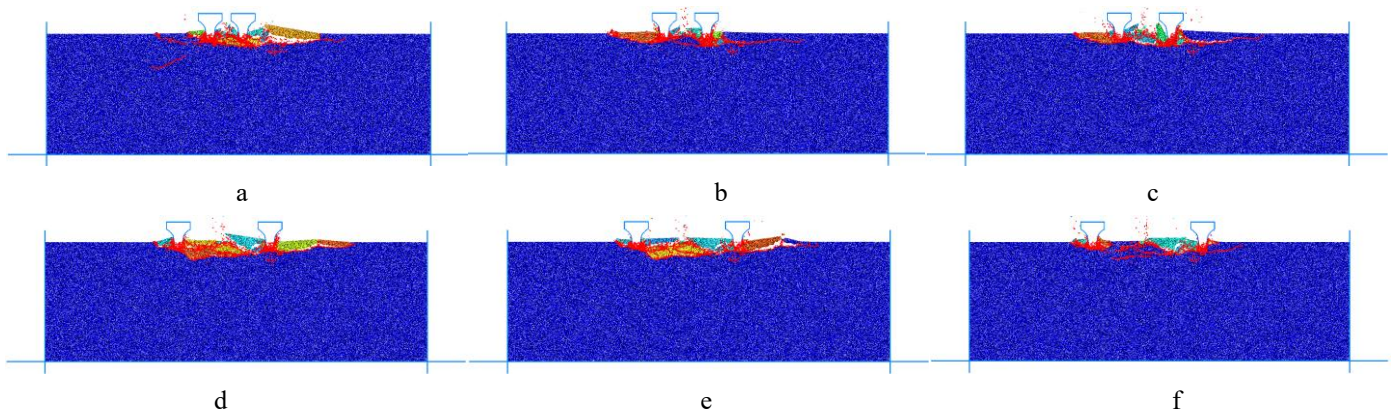


Fig. 21. Crack distribution at different cutter spacing for waveguide spacing of 150 mm: (a) cutter spacing: 70mm; (b) cutter spacing: 90mm; (c) cutter spacing: 110mm; (d) cutter spacing: 190mm; (e) cutter spacing: 210mm; (f) cutter spacing: 230mm.

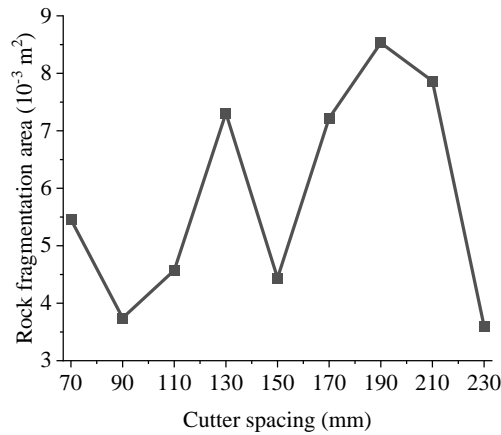


Fig. 22. The change curve of rock fragmentation area at different cutter spacing for waveguide spacing of 150mm.

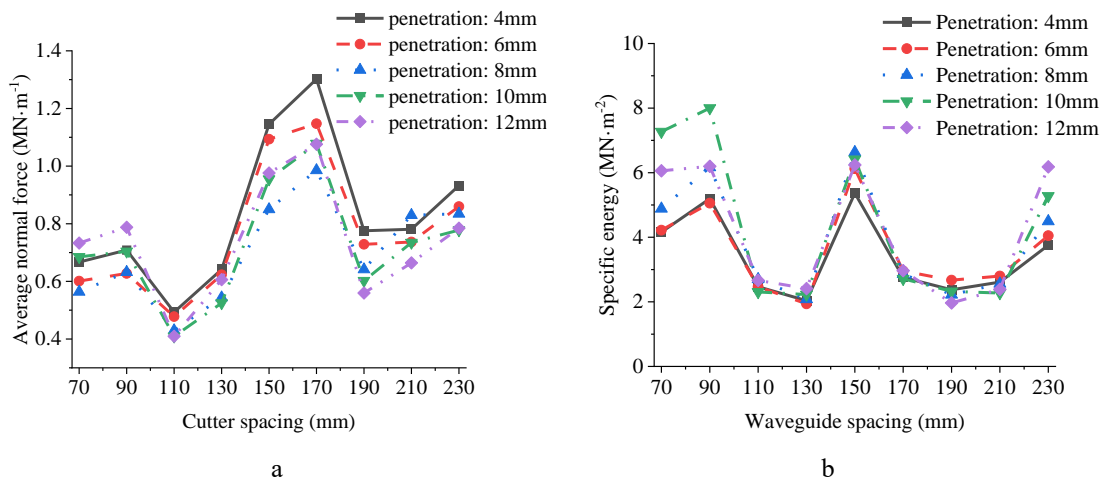


Fig. 23. The change curves of average normal force and specific energy at different cutter spacings for waveguide spacing of 150 mm: (a) the change curves of average normal force; (b) the change curve of rock-breaking specific energy.

4. Discussion

The positional relationship between microwave radiation and disc cutter rock-breaking penetration has a significant effect on the rock-breaking efficiency, which is an important reference value for the design of the mechanical arrangement of microwave-assisted TBM disc cutter rock-breaking technology. The results of the simulation study show that the maximum increase in the area of broken rock for a double-edged cutter with a cutter spacing of 180 mm in the range of 12 mm penetration before and after the microwave radiation is 138.57%, and the maximum decrease in the average normal force and the specific energy of rock-breaking is 77.84% and 87.23%, respectively. Lu et al. [57] used the power of 2.1kW microwave radiation Chifeng basalt, and the use of the reduced-scale SP3-I TBM cutter to complete the rock-breaking test research, the results show that microwave radiation makes the rock-breaking

volume increased significantly, disc cutter force and rock-breaking specific energy significantly reduced. Through comparative analysis, the simulation study has the same rule of change before and after microwave radiation, but due to the adjustment of microwave power and radiation time makes the input of microwave energy change, and the improvement effect in the hob force, rock-breaking, and rock-breaking specific energy is different [63].

On this basis, the relative positional relationship between microwave radiation and hob penetration is further analyzed in this study. When the double-edged cutter breaks rock at three relative positions with different waveguide spacings, normal force, rock-breaking area, and rock-breaking specific energy all show different patterns of change. The average normal force of the double-edged cutter when breaking rock in the center position, outer position, and inner position all increased with the increase of waveguide spacing in the range of 12 mm

penetration. Among them, the average normal force of the double-edged cutter when the double-edged cutter penetrates in the inner position is always minimized. Combined with the characteristics of damage crack distribution, it can be seen that the double waveguides radiation rock, has damage cracks in the approximate center of the radiation area, and along the perpendicular to the direction of the double-edged cutter penetration to the surface of the rock. This is because microwave radiation makes the temperature distribution of the rock decrease from the thermal core to the outside, forming the "inner compression, outer tensile" stress distribution [64], while the compressive strength of the rock is higher than the tensile strength, and the maximum temperature does not reach the rock pressure damage or melt damage temperature standard, so in the microwave radiation on both sides of the thermal core area produces tension-type fracture cracks, while in the microwave radiation on both sides of the thermal core area produces tension-type fracture cracks. type fracture cracks on both sides of the thermal core area of microwave radiation, while no crack penetration was formed at the thermal core. When a double-edged cutter breaks rock in the inner position, the thermal core area is not contained within the area between disc cutters. As a result, the average normal force required to break the rock is lower compared to the center and outer positions. When the double-edged cutter penetrates 12 mm in three relative positions, the waveguide spacing increases in a certain range to promote the increase of rock-breaking area. When the waveguide spacing is 90mm, the double-edged cutter reaches the maximum rock-breaking area of $6.802 \times 10^{-3} \text{ m}^2$ in the center position; when the waveguide spacing is 150mm, the double-edged cutter reaches the maximum rock-breaking area of $7.307 \times 10^{-3} \text{ m}^2$ and $7.221 \times 10^{-3} \text{ m}^2$ in the inner position and outer position, respectively; When the waveguide spacing continues to increase, although it can produce longer lateral cracks, there are deficiencies in the width and depth of rock breakage, resulting in relatively poor rock fragmentation and a gradual decrease in the rock-breaking area. This law is consistent with the results of Lu et al. [34] and Hartlieb et al. [58] for the effect of microwave radiation affecting rock-breaking by disc cutter. The rock-breaking efficiency of different positions is analyzed according to the calculation of rock-breaking specific energy, and it is shown that the center position reaches the minimum rock-

breaking specific energy when the waveguide spacing is 90 mm; the inner outer and outer positions reach the minimum rock-breaking specific energy when the waveguide spacing is 150 mm.

To further investigate the optimal arrangement of microwave and double-edged cutter, a double-edged cutter with different cutter spacing and double waveguides with 150 mm spacing were used to study the joint rock-breaking. The results show that the average normal force of the double-edged cutter, the area of the broken rock mass, and the specific energy of rock-breaking all show upward and downward oscillatory changes with the increase of the cutter spacing under the influence of microwave radiation. When the cutter spacing is 110mm to achieve the minimum average normal force; when the cutter spacing is 130mm to achieve the minimum rock-breaking specific energy; when the cutter spacing is 190mm to achieve the maximum rock-breaking area, and to a certain extent can reduce the amount of cutting tools. Considering the comprehensive rock-breaking efficiency and economic benefits, when deciding the cutter spacing, it should be selected according to the specific conditions and actual needs of engineering applications.

The study for microwave radiation simulation study is based on the assumption that microwave energy are absorbed by the rock minerals within the radiation range and generate heat energy to cause damage, is an ideal state of the simulation model. In practical engineering applications, microwave energy loss must exist, and the loss rate and engineering geological environment, mineral absorption capacity, waveguide radiation location and other factors are closely related. Therefore, in-depth research in combination with the actual working conditions needs to fully consider the influence of related factors. In addition, this study on the positional relationship between microwave radiation and double-edged cutter penetration also lacks the exploration of microwave radiation parameters, waveguide size, rock type and disc cutter type and other variables, and the application of microwave-assisted TBM disc cutter rock-breaking technology is still to be explored in depth.

5. Conclusions

To investigate the influence of the positional relationship

between microwave and double-edged cutter on the rock-breaking effect, the study uses the discrete element procedure (PFC) to establish a microwave-assisted double-edged cutter rock-breaking model based on the temperature change, strength damage, and cracking characteristics of granite before and after the microwave. Taking the double-edged cutter load, crack extension, and rock-breaking efficiency as the research indexes, the three relative positions of the double-edged cutter at different waveguide spacing are explored while analyzing the microwave-assisted improvement of the rock-breaking effect. Given the results of the relative position, a double-edged cutter with different spacing and a double waveguides with a spacing of 150mm are used for joint rock-breaking to deeply explore the optimal position of microwave and double-edged cutter action, yielding the following main findings:

(1) Comparative analysis of the rock-breaking effect of a double-edged cutter in the center position before and after microwave radiation reveals that microwave radiation produces lateral cracks perpendicular to the penetration direction of the double-edged cutter, which has a significant effect on the increase of the rock-breaking area, the decrease of the average normal force of the double-edged cutter and the rock-breaking specific energy. The maximum increase in the rock-breaking area of the double-edged cutter Within a cutter spacing of 180 mm is 138.57% when the double-edged cutters penetrates 12mm before and after the microwave radiation, and the maximum decrease in the average normal force and rock-breaking specific energy is 77.84% and 87.23%, respectively.

(2) The positional relationship between microwave radiation and double-edged cutter penetration has a significant effect on rock-breaking effectiveness. When the double-edged cutter breaks rock-breaking in three relative positions, the average normal force of the double-edged cutter increases with the increase of waveguide spacing, and the average normal force of

the double-edged cutter in the inner position is always smaller than that in the center position and the outer position; the area of rock-breaking with the increase of waveguide spacing shows the trend of "increasing first and then decreasing later" and reaches the maximum in the center position at waveguide spacing of 90mm; the maximum in the inner position and the outer position at waveguide spacing of 150mm; the specific energy of rock-breaking with the waveguide spacing of 150mm; and the maximum in the inner and outer positions at waveguide spacing of 150mm. The rock-breaking specific energy shows a trend of "decreasing first and then increasing" with the increase of waveguide spacing, and the center position reaches the minimum rock-breaking specific energy when the waveguide spacing is 90mm, and the inner position and outer position reach the minimum rock-breaking specific energy when the waveguide spacing is 150mm. The center position reaches the minimum breaking specific energy when the waveguide spacing is 90mm; the inner and outer positions reach the minimum breaking specific energy when the waveguide spacing is 150mm.

(3) When the waveguide spacing is 150mm, the average normal force of the double-edged cutter, the area of rock-breaking and the rock-breaking specific energy all show up and down oscillating trends with the increase of the cutter spacing. The minimum average normal force is achieved when the cutter spacing of 110mm is selected; the minimum rock-breaking specific energy is achieved when the cutter spacing of 130mm is selected; the maximum rock-breaking area is achieved when the cutter spacing of 190mm is selected and the total number of disc cutter equipped in the cutter plate is the smallest. Considering the comprehensive rock-breaking efficiency and economic benefits, the optimal cutter spacing needs to be selected according to the specific conditions and actual needs of engineering applications.

References

1. Editorial Department of China Journal of Highway and Transport. Review on China's Traffic Tunnel Engineering Research: 2022[J]. China Journal of Highway and Transport, 2022, 35(4): 1-40.
2. Entacher M, Lorenz S, Galler R. Tunnel boring machine performance prediction with scaled rock cutting tests[J]. International Journal of Rock Mechanics and Mining Sciences, 2014, 70: 450-459. <https://doi.org/10.1016/j.ijrmms.2014.04.021>
3. Rostami J. Performance prediction of hard rock Tunnel Boring Machines (TBMs) in difficult ground[J]. Tunnelling and Underground Space Technology, 2016, 57: 173-182. <https://doi.org/10.1016/j.tust.2016.01.009>
4. LIU P, LIANG W H. Design considerations for construction of the Qinling Tunnel using TBM [J]. Tunnelling and Underground Space

- Technology, 2000, 15(2): 139–146. DOI: 10.1016/S0886-7798(00)00041-9.
5. Su W, Li X, Jin D, et al. Analysis and prediction of TBM disc cutter wear when tunneling in hard rock strata: a case study of a metro tunnel excavation in Shenzhen, China[J]. *Wear*, 2020, 446: 203190
 6. VANIN D. The application of a tunnel-boring machine for exploration drifting at Kiena Gold Mines Limited, Val d'Or, Quebec [J]. *CIM Bulletin*, 1987, 80: 41–47.
 7. ROBBINS. Caving hard rock with a small diameter double shield [OL/OB]. The Robbins Company, 2014.http://www.therobbinscompany.com/wp-content/uploads/2014/09/Robbins_Newsletter_Summer_2014.pdf.
 8. Courbon C, Kramar D, Krajnik P, et al. Investigation of machining performance in high-pressure jet assisted turning of Inconel 718: an experimental study[J]. *International Journal of Machine Tools and Manufacture*, 2009, 49(14): 1114-1125. <https://doi.org/10.1016/j.ijmachtools.2009.07.010>
 9. Ayed Y, Germain G. High-pressure water-jet-assisted machining of Ti555-3 titanium alloy: investigation of tool wear mechanisms[J]. *The International Journal of Advanced Manufacturing Technology*, 2018, 96: 845-856. <https://doi.org/10.1007/s00170-018-1661-2>
 10. Carstens J P, Brown C O. Rock cutting by laser[C]//SPE Annual Technical Conference and Exhibition?. SPE, 1971: SPE-3529-MS.
 11. Xu Z, Reed C B, Konercki G, et al. Specific energy for pulsed laser rock drilling[J]. *Journal of laser applications*, 2003, 15(1): 25-30. <https://doi.org/10.2351/1.1536641>
 12. Dhar N R, Kamruzzaman M, Khan M M A, et al. Effects of cryogenic cooling by liquid nitrogen jets on tool wear, surface finish and dimensional deviation in turning different steels[J]. *International Journal of Machining and Machinability of Materials*, 2006, 1(1): 115-131. <https://doi.org/10.1504/IJMMM.2006.010662>
 13. Zhang S, Huang Z, Li G, et al. Numerical analysis of transient conjugate heat transfer and thermal stress distribution in geothermal drilling with high-pressure liquid nitrogen jet[J]. *Applied Thermal Engineering*, 2018, 129: 1348-1357. <https://doi.org/10.1016/j.applthermaleng.2017.10.042>
 14. Zhang J, Yang F, Cao Z, et al. In situ experimental study on TBM excavation with high-pressure water-jet-assisted rock-breaking[J]. *Journal of Central South University*, 2022, 29(12): 4066-4077. <https://doi.org/10.1007/s11771-022-5204-5>
 15. Rui F, Zhao G F. Experimental and numerical investigation of laser-induced rock damage and the implications for laser-assisted rock cutting[J]. *International Journal of Rock Mechanics and Mining Sciences*, 2021, 139: 104653.
 16. Dai X, Huang Z, Wu X, et al. Failure analysis of high-temperature granite under the joint action of cutting and liquid nitrogen jet impingement[J]. *Rock Mechanics and Rock Engineering*, 2021, 54(12): 6249-6264. <https://doi.org/10.1007/s00603-021-02600-1>
 17. Clark D E, Folz D C, West J K. Processing materials with microwave energy[J]. *Materials Science and Engineering: A*, 2000, 287(2): 153-158. [https://doi.org/10.1016/S0921-5093\(00\)00768-1](https://doi.org/10.1016/S0921-5093(00)00768-1)
 18. Kutlu N, Pandiselvam R, Saka I, et al. Impact of different microwave treatments on food texture[J]. *Journal of Texture Studies*, 2022, 53(6): 709-736. <https://doi.org/10.1111/jtxs.12635>
 19. Pandiselvam R, Hebbar K B, Manikantan M R, et al. Microwave treatment of coconut inflorescence Sap (Kalparasa®): A panacea to preserve quality attributes[J]. *Sugar Tech*, 2020, 22: 718-726. <https://doi.org/10.1007/s12355-020-00828-9>
 20. Lal A M N, Prince M V, Kothakota A, et al. Pulsed electric field combined with microwave-assisted extraction of pectin polysaccharide from jackfruit waste[J]. *Innovative Food Science & Emerging Technologies*, 2021, 74: 102844.
 21. Srinivas Y, Mathew S M, Kothakota A, et al. Microwave assisted fluidized bed drying of nutmeg mace for essential oil enriched extracts: An assessment of drying kinetics, process optimization and quality[J]. *Innovative Food Science & Emerging Technologies*, 2020, 66: 102541.
 22. Pandiselvam R, Prithviraj V, Manikantan M R, et al. Central composite design, Pareto analysis, and artificial neural network for modeling of microwave processing parameters for tender coconut water[J]. *Measurement: Food*, 2022, 5: 100015.
 23. Jones D A, Kingman S W, Whittles D N, et al. Understanding microwave assisted breakage[J]. *Minerals engineering*, 2005, 18(7): 659-669. <https://doi.org/10.1016/j.mineng.2004.10.011>
 24. Hartlieb P, Leindl M, Kuchar F, et al. Damage of basalt induced by microwave irradiation[J]. *Minerals Engineering*, 2012, 31: 82-89. <https://doi.org/10.1016/j.mineng.2012.01.011>
 25. Ford J D, Pei D C T. High temperature chemical processing via microwave absorption[J]. *Journal of Microwave Power*, 1967, 2(2): 61-64.

<https://doi.org/10.1080/00222739.1967.11688647>

26. Lu G, Li Y, Hassani F, et al. The influence of microwave irradiation on thermal properties of main rock-forming minerals[J]. *Applied Thermal Engineering*, 2017, 112: 1523-1532. <https://doi.org/10.1016/j.applthermaleng.2016.11.015>
27. Zheng Y L, Zhao X B, Zhao Q H, et al. Dielectric properties of hard rock minerals and implications for microwave-assisted rock fracturing[J]. *Geomechanics and Geophysics for Geo-Energy and Geo-Resources*, 2020, 6(1): 22. <https://doi.org/10.1007/s40948-020-00147-z>
28. Ali A Y, Bradshaw S M. Bonded-particle modelling of microwave-induced damage in ore particles[J]. *Minerals Engineering*, 2010, 23(10): 780-790. <https://doi.org/10.1016/j.mineng.2010.05.019>
29. Chen S, Yang C, Wang G. Evolution of thermal damage and permeability of Beishan granite[J]. *Applied Thermal Engineering*, 2017, 110: 1533-1542. <https://doi.org/10.1016/j.applthermaleng.2016.09.075>
30. Gautam P K, Verma A K, Sharma P, et al. Evolution of thermal damage threshold of Jalore granite[J]. *Rock Mechanics and Rock Engineering*, 2018, 51: 2949-2956. <https://doi.org/10.1007/s00603-018-1493-2>
31. Lu G M, Feng X T, Li Y H, et al. Experimental investigation on the effects of microwave treatment on basalt heating, mechanical strength, and fragmentation[J]. *Rock Mechanics and Rock Engineering*, 2019, 52: 2535-2549. <https://doi.org/10.1007/s00603-019-1743-y>
32. Sun H, Sun Q, Deng W, et al. Temperature effect on microstructure and P-wave propagation in Linyi sandstone[J]. *Applied Thermal Engineering*, 2017, 115: 913-922. <https://doi.org/10.1016/j.applthermaleng.2017.01.026>
33. Gao M Z, Yang B G, Xie J, et al. The mechanism of microwave rock-breaking and its potential application to rock-breaking technology in drilling[J]. *Petroleum Science*, 2022, 19(3): 1110-1124. <https://doi.org/10.1016/j.petsci.2021.12.031>
34. Lu G M, Feng X T, Li Y H, et al. The microwave-induced fracturing of hard rock[J]. *Rock Mechanics and Rock Engineering*, 2019, 52: 3017-3032. <https://doi.org/10.1007/s00603-019-01790-z>
35. Hartlieb P, Kuchar F, Moser P, et al. Reaction of different rock types to low-power (3.2 kW) microwave irradiation in a multimode cavity[J]. *Minerals Engineering*, 2018, 118: 37-51. <https://doi.org/10.1016/j.mineng.2018.01.003>
36. Peinsitt T, Kuchar F, Hartlieb P, et al. Microwave heating of dry and water saturated basalt, granite and sandstone[J]. *International Journal of Mining and Mineral Engineering*, 2010, 2(1): 18-29. <https://doi.org/10.1504/IJMME.2010.031810>
37. Zeng J, Hu Q, Chen Y, et al. Experimental investigation on structural evolution of granite at high temperature induced by microwave irradiation[J]. *Mineralogy and Petrology*, 2019, 113: 745-754. <https://doi.org/10.1007/s00710-019-00681-z>
38. Hartlieb P, Toifl M, Kuchar F, et al. Thermo-physical properties of selected hard rocks and their relation to microwave-assisted comminution[J]. *Minerals Engineering*, 2016, 91: 34-41. <https://doi.org/10.1016/j.mineng.2015.11.008>
39. Bisai R, Palaniappan S K, Pal S K. Influence of individual and combined pre-treatment on the strength properties of granite and sandstone[J]. *Arabian Journal of Geosciences*, 2020, 13: 1-10. <https://doi.org/10.1007/s12517-019-5009-5>
40. Deyab S M, Rafezi H, Hassani F, et al. Experimental investigation on the effects of microwave irradiation on kimberlite and granite rocks[J]. *Journal of Rock Mechanics and Geotechnical Engineering*, 2021, 13(2): 267-274. <https://doi.org/10.1016/j.jrmge.2020.09.001>
41. Nejati H, Hassani F, Radziszewski P. Experimental investigation of fracture toughness reduction and fracture development in basalt specimens under microwave illumination[M]//*Earth and Space 2012: Engineering, Science, Construction, and Operations in Challenging Environments*. 2012: 325-334. <https://doi.org/10.1061/9780784412190.036>
42. Kahraman S, Canpolat A N, Fener M. The influence of microwave treatment on the compressive and tensile strength of igneous rocks[J]. *International Journal of Rock Mechanics and Mining Sciences*, 2020, 129: 104303.
43. Zheng Y, Ma Z, Zhao X, et al. Experimental investigation on the thermal, mechanical and cracking behaviours of three igneous rocks under microwave treatment[J]. *Rock Mechanics and Rock Engineering*, 2020, 53: 3657-3671. <https://doi.org/10.1007/s00603-020-02135-x>
44. Li Q, Li X, Yin T. Effect of microwave heating on fracture behavior of granite: An experimental investigation[J]. *Engineering Fracture Mechanics*, 2021, 250: 107758. <https://doi.org/10.1016/j.engfracmech.2021.107758>
45. Lu G, Ding C, Hong K, et al. Influences of Microwave Irradiation on the Physicomechanical Properties and Cerchar Abrasivity Index of Rocks[J]. *Geofluids*, 2023, 2023. <https://doi.org/10.1155/2023/3889083>
46. Ge Z, Sun Q, Xue L, et al. The influence of microwave treatment on the mode I fracture toughness of granite[J]. *Engineering Fracture Mechanics*, 2021, 249: 107768. <https://doi.org/10.1016/j.engfracmech.2021.107768>

47. Yang Z, Yin T, Wu Y, et al. Mixed - mode I/II fracture properties and failure characteristics of microwave - irradiated basalt: An experimental study[J]. *Fatigue & Fracture of Engineering Materials & Structures*, 2023, 46(3): 814-834. <https://doi.org/10.1111/ffe.13897>
48. Bai G, Sun Q, Jia H, et al. Variations in fracture toughness of SCB granite influenced by microwave heating[J]. *Engineering Fracture Mechanics*, 2021, 258: 108048. <https://doi.org/10.1016/j.engfracmech.2021.108048>
49. Ahmadihosseini A, Shadi A, Rabiei M, et al. Computational study of microwave heating for rock fragmentation; model development and validation[J]. *International Journal of Thermal Sciences*, 2022, 181: <https://doi.org/10.1016/j.ijthermalsci.2022.107746>.
50. Hassani F, Shadi A, Rafezi H, et al. Energy analysis of the effectiveness of microwave-assisted fragmentation[J]. *Minerals Engineering*, 2020, 159: 106642. <https://doi.org/10.1016/j.mineng.2020.106642>
51. Teimoori K, Cooper R. Multiphysics study of microwave irradiation effects on rock breakage system[J]. *International Journal of Rock Mechanics and Mining Sciences*, 2021, 140: <https://doi.org/10.1016/j.ijrmms.2020.104586>
52. Shadi A, Ahmadihosseini A, Rabiei M, et al. Numerical and experimental analysis of fully coupled electromagnetic and thermal phenomena in microwave heating of rocks[J]. *Minerals Engineering*, 2022, 178: <https://doi.org/10.1016/j.mineng.2022.107406>.
53. GAO Feng, SHAO Yan, XIONG Xin, ZHOU Ke-ping, CAO Shan-peng. Rising characteristics of internal and external temperatures of rock specimens under different microwave irradiation modes[J]. *Chinese Journal of Geotechnical Engineering*, 2020, 42(4): 650-657. doi: 10.11779/CJGE202004007
54. Feng X, Li S, Yang C, et al. The Influence of the Rotary Speed of a Microwave Applicator on Hard-Rock Fracturing Effect[J]. *Rock Mechanics and Rock Engineering*, 2022, 55(11): 6963-6979. <https://doi.org/10.1007/s00603-022-02956-y>
55. Rui F, Zhao G F, Zheng Y, et al. Electromagnetic-thermo-mechanical coupled modelling of microwave-assisted TBM disc cutting[J]. *Tunnelling and Underground Space Technology*, 2023, 138: <https://doi.org/10.1016/j.tust.2023.105171>.
56. Lu G, Zhou J, Zhang L, et al. Experimental investigation on the influence of microwave exposure on the cutting performance of TBM disc cutter cutting of hard rocks[J]. *Results in Engineering*, 2021, 12: <https://doi.org/10.1016/j.tust.2023.105171>.
57. Lu G, Ding C, Zhou J, et al. Influences of Microwave Irradiation on Rock-Breaking Efficiency of a Reduced-Scale TBM Cutter[J]. *Applied Sciences*, 2023, 13(8): 4713. <https://doi.org/10.3390/app13084713>
58. Hartlieb P, Grafe B, Shepel T, et al. Experimental study on artificially induced crack patterns and their consequences on mechanical excavation processes[J]. *International Journal of Rock Mechanics and Mining Sciences*, 2017, 100: 160-169. <https://doi.org/10.1016/j.ijrmms.2017.10.024>
59. Marland S, Merchant A, Rowson N. Dielectric properties of coal. *Fuel*. 2001;80(13):1839-49. [https://doi.org/10.1016/S0016-2361\(01\)00050-3](https://doi.org/10.1016/S0016-2361(01)00050-3)
60. Jones DS. *The theory of electromagnetism*. Oxford: Pergamon Press; 1964.
61. Itasca. PFC2D—Particle Flow Code in 2 Dimensions, Version 5.0 [M]. Itasca Consulting Group Inc. Minneapolis, MN, USA, 2014.
62. Hassani F, Nekoovaght P M, Gharib N. The influence of microwave irradiation on rocks for microwave-assisted underground excavation[J]. *Journal of Rock Mechanics and Geotechnical Engineering*, 2016, 8(1): 1-15. <https://doi.org/10.1016/j.jrmge.2015.10.004>
63. Hartlieb P, Grafe B. Experimental study on microwave assisted hard rock cutting of granite[J]. *BHM Berg-und Hüttenmännische Monatshefte*, 2017, 162(2): 77-81. <https://doi.org/10.1007/s00501-016-0569-0>
64. Wang J., Feng C., Zhang Y. Numerical simulation of rock thermal fracture considering the temperature dependence[J]. *Journal of Shandong University(Engineering Science)*, 2023, 53(1): 106-113.